archives
of thermodynamics
Vol. **43**(2022), No. 3, 141–173
DOI: 10.24425/ather.2022.143176

Novel model for emptying of a self-pressurised nitrous oxide tank

JAKUB SZYMBORSKI*
DARIUSZ KARDAŚ

The Szewalski Institute of Fluid Flow Machinery, Polish Academy of Sciences, Fiszera 14, 80-231 Gdańsk, Poland

Abstract Nitrous oxide is often used in the space industry, as an oxidiser or monopropellant, mostly in self-pressurised configurations. It has potential for growth in use due to the recent rising interest in green propellants. At the same time, modelling the behaviour of a self-pressurising nitrous oxide tank is a challenging task, and few accurate numerical models are currently available. Two-phase flow, heat transfer and rapid changes of mass and temperature in the investigated system all increase the difficulty of accurately predicting this process. To get a get better understanding of the emptying of a self-pressurised nitrous oxide tank, two models were developed: a phase equilibrium model (single node equilibrium), treating the control volume as a single node in equilibrium state, and a phase interface model, featuring a moving interface between parts of the investigated medium. The single node equilibrium model is a variation of equilibrium model previously described in the literature, while the phase interface model involves a novel approach. The results show that the models are able to capture general trends in the main parameters, such as pressure or temperature. The phase interface model predicts nitrous oxide as a liquid, a two-phase mixture, and vapour in the lower part of the tank, which is reflected in the dynamics of changes in pressure and mass flow rate. The models developed for self-pressurisation, while created for predicting nitrous oxide behaviour, could be adapted for other media in conditions near vapour–liquid equilibrium by adding appropriate state equations.

Keywords: Convective mass transfer; Nitrous oxide; Hybrid rocket engine; Two-phase flow; Self-pressurisation

*Corresponding Author. Email: jszymborski@imp.gda.pl

Nomenclature

A	–	area
$A_{\mathrm{dia\_in}}$	–	tank inner cross-sectional area
Cd	–	discharge coefficient
CdA	–	numerical coefficient combining discharge coefficient and area
C_{db}	–	average bubble drag coefficient
c_w	–	tank specific heat
E	–	empirical factor
h	–	enthalpy
$\dot{m}$	–	mass flow rate
$\dot{m}_{\mathrm{rise}}$	–	mass flow rate of vapour rising bubbles
$\dot{m}_{\mathrm{out}}$	–	mass outflow rate
Ma	–	Mach number
P	–	pressure
h	–	enthalpy
h_e	–	phase change enthalpy
$\dot{Q}$	–	heat flux
$\dot{q}_s$	–	heat flux density
R	–	gas constant
Pr	–	Prandtl number
T	–	temperature
t	–	time
v	–	velocity
V	–	volume

Greek symbols

α	–	volumetric void fraction
μ	–	dynamic viscosity
ρ	–	density

Subscripts and superscripts

b	–	bottom, regarding bottom node of a model
bubble	–	regarding bubble / vapour stream from a bottom node
cv	–	condensing vapour
ev	–	evaporating
liq	–	liquid
s	–	from saturation line
u	–	upper, regarding upper node of a model
v	–	vapour
w	–	tank wall

Acronyms

CFD	–	computational fluid dynamics
CP	–	Casalino-Pastrone two-phase lumped parameter model
EQ	–	Zakirov-Li equilibrium model
MAE	–	mean absolute error

PIM	–	phase interface model
SNE	–	single node equilibrium
SPI-HEM	–	single phase incompressible-homogeneous equilibrium model
ZK	–	Zilliac-Karabeyoglu real fluid, quasi-phase equilibrium model

1 Introduction

Nitrous oxide is used in the space industry, particularly in hybrid rockets as an oxidiser [1–3], and is considered as a potential monopropellant for satellite thrusters [4, 5]. Its main advantages are nontoxicity, low cost, market availability, and ease of storage at a wide range of temperatures.

Further advantages are apparent when it is used as an oxidiser in hybrid rocket engines. A typical small-scale rocket motor using a liquid oxidiser such as oxygen requires a pressurising system. It is needed to maintain a high tank pressure to ensure the desired pressure head and therefore the desired mass flow of the oxidiser. If the fluid used has high saturation pressure, it is possible to omit the pressurising system and make the medium pressurise itself. While oxygen has a critical point at a vapour pressure of 5 MPa and a temperature of 155 K (−118°C), nitrous oxide has a critical point at pressure of 7.2 MPa and a temperature of 310 K (37°C). This means that nitrous oxide can be kept liquid within a pressurised tank at room temperature, while storing liquid oxygen requires cryogenic temperatures. As a result, nitrous oxide can remain at high pressure without additional pressurisation by boiling if the pressure drops, and is therefore self-pressurising. In this case, nitrous oxide can remain in vapour-liquid equilibrium up to 310 K. These properties may be utilised in the design of an effective and lightweight oxidiser feeding system, removing the need for cryogenic tanks and/or additional pressurisation. While using self-pressurisation offers simple hardware design, it also increases the difficulty of modelling, with complex physical phenomena such as evaporation, boiling, heat transfer and two-phase flow having a significant impact on the system's characteristics. Due to this complexity, there are few robust numerical models, and those available are incapable of predicting the transient flow features occurring during the emptying of a self-pressurised nitrous oxide tank. The goal of this study is to the investigate possibility of developing a fast and accurate numerical model of a self-pressurising nitrous oxide tank, for application in the prototyping and optimisation of systems using such tanks, particularly for hybrid rocket engines.

1.1 Existing models

Winter and Marchetta [1] used computational fluid dynamics (CFD) to investigate the influence of external heat flux, namely the impact of solar radiation, on heating the spacecraft tanks. Cryogenic storage tanks on spacecraft are subjected to heating by solar radiation over long periods of time during space flight. Heating results in pressure increase due to self-pressurisation. Such pressure increase, if not controlled, might lead to rupture of the tanks and it is therefore important to predict rises in pressure. The cited authors used a pressure-based model with the application of an energy of fluid method to simulate this phenomenon. The case with the refrigerant R-12 was used as a benchmark, and revealed a need for further studies on simulation parameters, such as relaxation factor, time step size and mesh cell size.

Analysis of a self-pressurising tank under heat influx was carried out using CFD in [7]. Hydrogen under normal and microgravity was simulated using Ansys Fluent, using volume of fluid method, allowing for tracking of the phase interface. The authors analysed impact of varying number of layers of insulation on heat influx and speed of evaporation of initially liquid hydrogen. Comparison with experimental results was not shown, although results prove that commercially available software could be used for handling a self-pressurising fluid tank.

Apart from CFD simulations, there have been several other approaches, both simpler and more tailored to the modelling of self-pressurisation. One commonly used approach is to use a lumped parameter (or element) model. Such a model simplifies the description of a real life system by assuming that a certain part of the system can be treated as uniform element, such as the tank walls, or fluid stored within the tank. Such an element, or node of the model, therefore has one temperature, one mass, etc. By defining interactions between the elements, the whole system may be modelled. For example, heat transfer between the tank wall and fluid within the tank might be reduced to a single differential equation.

In the literature there are several lumped parameter models developed for the modelling of self-pressurised nitrous oxide. They feature varying levels of complexity, regarding both the state of the working medium and source terms for mass and heat transfers, depending on the desired depth of the model.

One type of such models is equilibrium models, which have been presented in the literature several times, for example by Casalino and Pas-

trone [8], and by Zakirov and Li [9]. The difference between these two models is that the former incorporates a heat transfer model, while the latter does not.

The equilibrium model (subsequently referred to as EQ) examined here was published by Zakirov and Li and later compared with other models in [10]. It features two separate calculation nodes, one for vapour and one for liquid, both in saturated state. It is assumed that changes due to the outflow are significantly slower than heat and mass transfer between phases within the tank, and therefore the nitrous oxide is always in phase equilibrium. Based on this assumption, mass and energy conservation equations can be written for the whole tank, removing the need for mass and heat transfer between the nodes. To add heat transfer between the tank walls and the fluid, two additional equations are needed to calculate the wall temperature in the parts in contact with the vapour phase and liquid phase.

Casalino and Pastrone [8], proposed two models, a simpler one, a variant of a homogeneous equilibrium model; and a more complex, two-phase lumped parameter model. Both are intended as a part of a hybrid rocket optimisation tool. The former will not be discussed as it is similar to the equilibrium model already described. The latter model, subsequently referred to as CP, consists of saturated vapour and superheated liquid with terms for mass transfer between them. The authors have started from the observation that during emptying, the medium within the tank is not in equilibrium. Instead, a temperature gradient exists, with warmer liquid and colder vapour. One can assume that within a single phase, the temperature is uniform. The mass stream due to condensation and evaporation was assumed to be a function of pressure, with each mass stream set to maintain saturation state within the vapour. As a result, four equations are solved for mass flux of liquid ($\dot{m}_{\mathrm{liq}}$), evaporating ($\dot{m}_{\mathrm{ev}}$) or condensing ($\dot{m}_{\mathrm{cv}}$) mass flux, and temperatures of vapour (T_v) and liquid (T_{liq}).

Zilliac and Karabeyoglu proposed a more refined model, which they described as a real fluid, quasi-phase equilibrium propellant tank model [11]. Their model (subsequently referred to as ZK) shares the lumped parameter approach with the EQ model, but uses a more detailed approach. The whole system is divided into fluid and solid parts. The fluid control volume consists of three elements, namely the vapour, the liquid, and the liquid surface layer from which evaporation occurs. The solid part of the control volume consists of the tank walls. Each of these elements has a separate temperature. For simplicity, the temperature of the liquid surface layer was assumed to be the saturation temperature, resulting in two fluid elements

and a single solid element. Heat transfer source terms include convective heat transfer between fluid elements, heat transfer due to phase changes, and heat transfer between respective fluid parts and the solid. Additionally, heat flux from the external environment and tank walls is also modelled. The division of the control volume into liquid and vapour creates a need for mass transfer modelling. Furthermore, the authors found that mass transfer between nodes due to evaporation was crucial for accurate process prediction. This was achieved by linking evaporation mass flux to heat transfer. First, the presence of a thin layer of saturated liquid on top of the liquid node is assumed. The layer acts as a buffer between nodes, which has thermal contact with both sides. If there is an imbalance in heat fluxes, then the difference determines mass flux evaporation or condensation. Since heat flux from the liquid side is calculated using relations designed for convection, it does not account for boiling, interface motion and blowing, and is therefore significantly underestimated. To account for this, the model adds an empirical factor E with order of magnitude of 10^3, designed to be later tuned to fit experimental results. This parameter directly multiplies the amount of heat transferred, and is used in the heat transfer equation.

As a result, the ZK model solves six equations to predict the mass and energy of both nodes as well as wall temperatures in the bottom and upper parts of the tank.

A comprehensive review and evaluation of the ZK, EQ, and CP models was published by Zimmerman *et al.* [10]. A data set containing four different experiments, including data used by the authors of the three reviewed models, was gathered and used for assessing the performance of the selected models. The accuracy of the investigated models was evaluated using pressure and temperature predictions and how those predictions reflect experimental measurements. For initial conditions, the initial pressure was used, along with either the mass or the fill level of fluid nitrous oxide within the tank. The experiments in question used different setups for emptying the tanks, including a feed line and injectors; the authors of the review therefore decided not to recreate flow through a feed line and injectors. Instead, each model was fitted using a numerical parameter CdA, serving as a parameter including both the size and type of injector setup. Typically, when modelling flow through an orifice, both the discharge coefficient (Cd) and cross-sectional area (A) are taken into account. In this case, both parameters were combined into one, adjustable parameter used to tune the model to experimental data.

Selection of this parameter was performed for each model and each experimental test individually based on the averaged mass flow. The averaged mass flow was assessed by the outflow time of the liquid part of nitrous oxide. Additionally, the ZK model features an empirical coefficient E, describing an additional multiplier for the heat transfer between the liquid and surface parts of the medium, which is dependent on the test setup. This coefficient was optimised in order to minimise the difference between the predicted and measured pressure.

As a result of this evaluation, several important points about the models under investigation were noted. The EQ model, being the simplest, shows the smallest number of features of the flow. It does not predict a sudden, initial pressure drop, and pressure decrease remains stable throughout the process. Despite this, general pressure trends were predicted accurately.

The CP model, which in terms of complexity is situated between the EQ and ZK models, fares poorly in comparison with the other models. According to the authors of the review, this might be caused by difference between the sources of thermodynamic properties used, which has a great potential impact on the accuracy of the calculations.

The ZK model, the most detailed of the three, unsurprisingly gives the most accurate results in the chosen test cases. At the same time, only the ZK model had an additional optimisation parameter adjusted in order to minimise the error of pressure prediction, namely the heat transfer multiplier E. The need for this parameter undermines the usability of this model for the prediction of flow parameters of new systems, which do not have this parameter specified.

To conclude, [10] presents an interesting and educating look at important lumped parameters models used for the simulation of self-pressurising nitrous oxide systems, but it is not without its own issues. As these models, being significantly simpler and less costly to use than CFD, are used mainly for preliminary design and optimization, it is important to investigate them in the context in which they are used. First, the simulations were limited to the part of the process with liquid-dominated flow, with the end condition set as the end of liquid flow. From the hybrid rocket engine standpoint, this covers most of the useful part of the flow, bearing the majority of the oxidiser mass. Nonetheless, the emptying process itself does not end until the tank pressure reaches equilibrium with downstream conditions. As was demonstrated in experiments with a transparent tank [12], after the liquid is evacuated, nitrous oxide vapour and condensed vapour remain within the tank, which may include a not insignificant amount of mass. By limiting the

investigated process to the moment at which the liquid is drained, ambiguity is introduced regarding the boundary conditions. First, while clear in the experiment with a transparent tank, in a numerical experiment it might be difficult to identify this moment correctly, especially if the assumptions allow the vapour part to be in non-saturated state. This further translates into difficulty determining the final pressure inside the tank, which may vary significantly, depending on the state of the remaining fluid.

Considering the current state of the models for self-pressurising media, the authors believe that is room for improvement in the modelling used. Key areas for investigation are heat and mass transfer processes occurring within the modelled systems, which to date have not been taken into account in a sufficiently detailed manner.

1.2 Available experimental findings

The complex nature of the behaviour of nitrous oxide in a self-pressurising tank during emptying requires detailed investigation. Small-scale experiments with nitrous oxide being evacuated into the atmosphere were conducted in [12]. The authors used a transparent cylinder, with pressure and temperature sensors fitted. The cylinder was filled with nitrous oxide up to a given level, and the pressure was allowed to stabilise over time. The experiment was started with the liquid fill level at around 90% of tank height, with the outlet at the bottom. All cases of self-pressurising tank emptying shared similar characteristic features, visible on pressure-time history plots: a sharp initial drop, a subsequent increase, and a steady, near-linear decrease. In the final part of the process, the rate of pressure drop was significantly increased until the end of the flow.

Photographic documentation enables the recorded changes in pressure to be associated with changes observed *via* optical access. First, as soon as the outflow valve had been opened, bubbles of vapour became observable, rising upwards from the bottom. After the bubble column had reached the top surface of the liquid nitrous oxide, the apparent amount of bubbles stabilised, with the bubbles' apparent distribution uniform across the liquid. During the next seconds of the experiment three separate regions became apparent: a cloud of condensed vapour in the top part, a transparent gas near above the liquid part, and in the bottom part a liquid with significant presence of bubbles. It is notable that the apparent amount of bubbles seemed to be constant throughout emptying, and that the boundary between the mostly-liquid part and the gaseous part was clearly visible.

The same characteristic features were observed in experiments with varying outflow valve settings.

Variation in temperature along the longitudinal axis of a self-pressurising tank was investigated in [13,14] using a set of thermocouples. Temperature profiles were recorded during tank filling and emptying. In both cases, it was observed that temperature variation within the liquid nitrous oxide is significantly smaller than within portion of the tank filled with vapour. In [13], tank filled up to pressure of 2.62 MPa had liquid temperature of approx. 265 K, with negligible temperature stratification, while temperature measurements within the gaseous part ranged from approx. 273 K to approx. 295 K, over distance of 0.4 m between respective thermocouples, resulting in temperature gradient in order of 55 K/m, measured immediately after end of the filling process.

In [14], during filling, temperatures within gas-filled portion of the tank varied from 291.2 K to 280.5 K, giving a gradient of 15.3 K/m, while within liquid-filled portion, temperatures varied from 276 K to 277 K, resulting in a temperature gradient of 4.4 K/m. After 30 min wait period, measured gradients were 10.2 K/m in vapour and 0.6 K/m in liquid.

Based on those results, it can be assessed that temperature within the liquid section of a self-pressurised tank is almost constant along height and can be therefore represented by a single computational node in a lumped-parameter approach. At the same time, within the section of a tank filled with vapour, there is a significant temperature gradient, which suggest that describing this part as a single element in a lumped-parameter approach introduces inaccuracy to such model.

2 Materials and methods

To gain broader experience and to propose a fresh approach in the modelling of a self-pressurising tanks, two new models were prepared, which are evolution of models described in [2]. Both use lumped parameters approach; in the first case, saturated two-phase mixture takes up the entire volume, while in the second case, the liquid and vapour nodes are separated by an interface.

2.1 Single node equilibrium model

The first model is similar to the equilibrium model reported in [3] and will be referenced as the single node equilibrium (SNE) model. The fluid is

assumed to be represented by a single node, being in the form of pure vapour or pure liquid or in a two phase state. Nitrous oxide fills the whole available volume of the tank, and is described by a single pressure p and single enthalpy h. In this approach, N_2O stays in the similar state through the whole process, where the oxidiser is a liquid–vapour mixture. Evaporation increases volume of vapour within the tank and is caused by a drop in pressure, which results from the outflow from the tank. The SNE model takes into account internal energy transfer to and from the tank. Like the oxidant, the tank walls are assumed to be a single entity from a thermal standpoint, and are described by a lumped parameter equation. In this model, energy exchange occurs between fluid phases and between nitrous oxide and the tank walls. It is further assumed that the mixture consists of liquid and vapour from the saturation line. A simplified schematic diagram of this model is shown in Fig. 1.

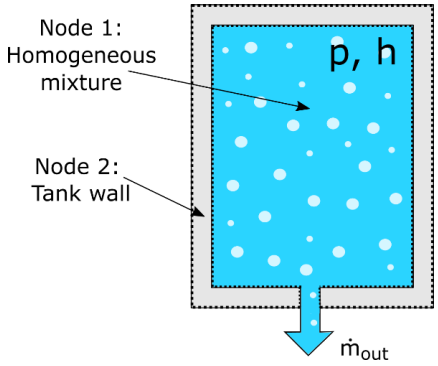

Figure 1: Schematic diagram of an oxidiser tank for the single node equilibrium model.

Given all these assumptions, the SNE model is described by three differential equations:

- fluid mass flux balance

$$V\frac{d\rho(p,h)}{dt} = -\dot{m}_{\text{out}}\,, \tag{1}$$

- fluid energy balance

$$V\frac{d\rho(p,h)h}{dt} = -\dot{m}_{\text{out}}h + \dot{Q}\,, \tag{2}$$

- tank energy balance

$$V_w c_w \frac{dT_w}{dt} = -\dot{Q}\,, \tag{3}$$

where V is the fluid volume in the tank, ϱ is the density, p the pressure and h the enthalpy of N_2O, $\dot{m}_{\text{out}}$ is the outflow mass flux, $\dot{Q}$ is the fluid–wall heat flux, V_w is the tank wall volume, c_w is the specific heat of the tank and T_w is the tank temperature. The model described in this way has three unknowns: fluid pressure p, enthalpy h, and tank wall temperature T_w.

Initial conditions are specified as:

$$p_0 = p(t=0), \qquad h_0 = h(t=0), \qquad T_{w0} = T_w(t=0). \tag{4}$$

2.2 Phase interface model

The second, more advanced model is called the phase interface model (PIM). The tank's inner volume is divided into two parts, or nodes: an upper part, intended to contain mostly vapour, and a bottom part, intended to contain mostly liquid or liquid-dominated mixture, as shown schematically in Fig. 2. An important feature of this model is the assumption of thermodynamic equilibrium in each part and thermodynamic non-equilibrium between them. In the both parts, liquid and vapour are assumed to be well mixed within the volume. The phase transition in the lower part is caused by the pressure drop, which results from mass outflow and from mass transfer on the interfacial surface separating the upper and bottom parts. The N_2O thermodynamic parameters also change as a result of heat exchange with the walls of the tank. A key feature of this proposed model is that it allows differentiation between the outflow of pure liquid, a two-phase mixture and N_2O vapour.

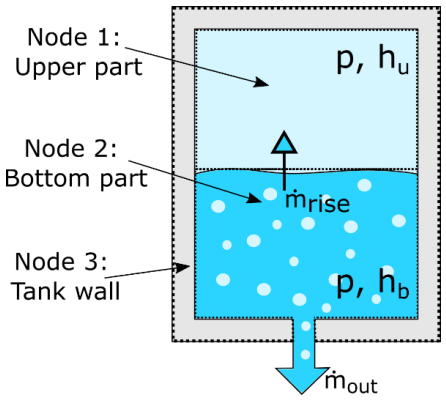

Figure 2: Schematic diagram of an oxidiser tank for the phase interface model.

As in the previous model, PIM is described by mass and energy equations for each part. This increases the degrees of freedom of the system and the possibility of more dynamic changes in the parameters. The novelty of this model is that the vapour bubbles rise in the lower part of the tank are taken into account. The vapour bubbles rise due to buoyancy force. Mass stream due to rising bubbles is denoted $\dot{m}_{\text{rise}}$, and is shown symbolically in Fig. 2. Mass and energy balances for the upper and bottom parts (four equations) and the tank wall energy balance are calculated according to Eqs. (5)–(9).

The upper part mass conservation equation is as follows:

$$\frac{d\alpha_u \rho_u(p, h_u)}{dt} = \dot{m}_{\text{rise}} \tag{5}$$

and the upper part energy conservation equation has the form

$$\frac{d\alpha_u \rho_u(p, h_u) h_u}{dt} = \dot{m}_{\text{rise}} h_v^s + \dot{Q}_u \,. \tag{6}$$

The fluid in the bottom part is an open system with two discharges of mass and energy, one caused by the rise of bubbles, the other by an outflow of the mixture. Therefore, the bottom part fluid mass conservation equation may be written

$$\frac{d\alpha_b \rho_b(p, h_b)}{dt} = -\dot{m}_{\text{rise}} - \dot{m}_{\text{out}} \tag{7}$$

and the energy equation takes the following form:

$$\frac{d\alpha_b \rho_b(p, h) h_b}{dt} = -\dot{m}_{\text{rise}} h_v^s - \dot{m}_{\text{out}} h_b + \dot{Q}_b \,. \tag{8}$$

The oxidiser tank volume is treated as a lumped element, hence its energy equation is given by

$$V_w c_w \frac{dT_w}{dt} = -\dot{Q}_u - \dot{Q}_b \,. \tag{9}$$

The model defined in this way, consisting of the above five equations, has five unknowns: pressure p, upper volumetric void fraction α_u, upper enthalpy h_u, bottom enthalpy h_b, and tank wall temperature T_w. The volumetric ratio of the bottom part is described as $\alpha_b = V_b/V$ where V_b is the bottom fluid volume. Vapour saturation enthalpy h_v^s is a function of pressure, $\dot{Q}_u$ and $\dot{Q}_b$ are heat fluxes between the walls and the upper and bottom element respectively, and V_w and c_w are the tank walls' volume and tank walls heat capacity.

To solve the numerical problem, boundary conditions are necessary. For PIM, they are specified as follows:

$$\begin{gathered} \alpha_{u0} = \alpha_u(t=0), \qquad p_0 = p(t=0), \qquad h_{u0} = h_u(t=0), \\ h_{b0} = h_b(t=0), \qquad T_{w0} = T_w(t=0). \end{gathered} \tag{10}$$

The density function in the balance Eqs. (1)–(2) and (5)–(8), when differentiated with respect to time, gives

$$\frac{d\rho(p,h)}{dt} = \left(\frac{\partial\rho}{\partial p}\right)_h \frac{dp}{dt} + \left(\frac{\partial\rho}{\partial h}\right)_p \frac{dh}{dt}. \tag{11}$$

The SNE and PIM model systems of equations requires thermodynamic functions of density and its derivatives. Because the fluid undergoes phase transitions, it is necessary to take into account the current phase of the fluid. In this context, the accuracy of the approximation of properties and their derivatives and the maintenance of their continuity in phase transition from a single-phase state to a two-phase mixture and *vice versa* play a significant role. The fluid phase is verified by comparing the current enthalpy h with the liquid $h^s_{\text{liq}}(p)$ and vapour $h^s_v(p)$ saturation enthalpy according to equation

$$\text{phase} = \begin{cases} \text{liquid}, & h \le h^s_{\text{liq}}(p), \\ \text{two-phase mix.}, & h^s_{\text{liq}}(p) < h < h^s_v(p), \\ \text{vapour}, & h \ge h^s_v(p). \end{cases} \tag{12}$$

The density function and density derivatives of pure liquid and vapour were approximated by different polynomials in terms of two variables p and h. Approximation data, i.e. density and density derivatives depending on pressure and enthalpy, were extracted from the *Reference Fluid Thermodynamic and Transport Properties Database* (REFROP) [16] for a range of applicable conditions. REFPROP was created and is continuously maintained by the National Institute of Standards and Technology (NIST) and features accurate models of thermophysical properties of a number of fluids, including nitrous oxide.

For the density of the two-phase mixture one can write

$$\rho(p,h) = \frac{1}{\dfrac{x(p,h)}{\rho^s_v(p)} + \dfrac{1-x(p,h)}{\rho^s_{\text{liq}}(p)}}, \tag{13}$$

where ρ_v^s and ρ_{liq}^s represent the densities of the vapour and liquid, and x is the vapour mass fraction. The vapour mass fraction can be expressed as a function of the enthalpy of the mixture h, saturation liquid enthalpy h_{liq}^s and saturation vapour enthalpy h_v^s.

$$x(p,h) = \frac{h - h_{\text{liq}}^s(p)}{h_v^s(p) - h_{\text{liq}}^s(p)}\,. \tag{14}$$

Using (13) and (14), the density derivative $(\partial\rho/\partial p)_h$ for the two-phase mixture has the following form:

$$\left(\frac{\partial\rho}{\partial p}\right)_h = \left(\frac{\partial\rho}{\partial\rho_{\text{liq}}^s}\right)_h \frac{d\rho_{\text{liq}}^s}{dp} + \left(\frac{\partial\rho}{\partial\rho_v^s}\right)_h \frac{d\rho_v^s}{dp} + \left(\frac{\partial\rho}{\partial x}\right)_{\rho_{\text{liq}}^s,\rho_v^s} \left[\left(\frac{\partial x}{\partial h_{\text{liq}}^s}\right)_{h,h_v^s} \frac{dh_{\text{liq}}^s}{dp} + \left(\frac{\partial x}{\partial h_v^s}\right)_{h,h_{\text{liq}}^s} \frac{dh_v^s}{dp}\right], \tag{15}$$

while for $(\partial\rho/\partial h)_p$ we have

$$\left(\frac{\partial\rho}{\partial h}\right)_p = \left(\frac{\partial\rho}{\partial x}\right)_{\rho_{\text{liq}}^s,\rho_v^s} \left(\frac{\partial x}{\partial h}\right)_{h_{\text{liq}}^s,h_v^s}. \tag{16}$$

An important element of the physical modelling in the PIM is mass transfer between nodes. After testing, comparison with experimental results, and examination of the available photographs of nitrous oxide in a transparent tank done available in [12], it was concluded that bubbles of vapour created within the liquid may be responsible for a significant portion of the mass transfer within the tank. To take account of that phenomenon, a source term for rising mass is proposed:

$$\dot{m}_{\text{rise}} = v_{\text{bubble}} \alpha_b^v A_{\text{dia\_in}} \rho_v^s\,, \tag{17}$$

where α_b^v is the volumetric measure of vapour within the bottom element, $A_{\text{dia\_in}}$ is the cross-sectional area of the tank, ρ_v^s is the vapour density at saturation conditions, and the bubble velocity v_{bubble} is calculated using, according to [17], equation

$$v_{\text{bubble}} = \sqrt{\frac{4gD_{\text{bubble}}\left(\rho_{\text{liq}}^s - \rho_v^s\right)}{3C_{\text{db}}\rho_{\text{liq}}^s}}\,, \tag{18}$$

where ρ^s_{liq} is saturated liquid density, ρ^s_v is saturated vapour density, g is the gravitational acceleration, D_{bubble} is average bubble diameter, and C_{db} is the average bubble drag coefficient. While parameters for this term such as saturation densities or void fraction are well defined within the model, parameters for calculating bubble velocity v_{bubble} have to be estimated. The drag coefficient for bubbles was estimated to be 0.44. Initially, average bubble diameter was assumed to be 0.2 mm.

Addition of the rising mass source term, which depends on the current state of fluid in the bottom parts, has impact on thermodynamics of the model. By adding mass and heat transfer between the nodes the model gains an extra degree of freedom, and causes the unknowns to be not only a function of pressure and enthalpy, but also a function of the newly introduced term.

In both developed models, heat transfer between the liquid-dominant part and the tank wall is assumed to be described by a nucleate boiling expression. This assumption is based on the experimental observations of the oxidiser in self-pressurising conditions during emptying, which shows the substantial presence of vapour bubbles. Since the tank walls are expected to be warmer than the fluid during outflow, it is reasonable to assume that the walls will promote the formation of bubbles and therefore the intensification of heat transfer in a manner similar to nucleate boiling. Obtaining an accurate estimate of heat transfer coefficient for such case would be a challenging and would require additional modelling, as shown by [4], for flow of carbon dioxide in similar conditions. Herein, this is described by equation defining heat flux density, according to [18],

$$\dot{q}_s = \mu_{\text{liq}} h_e \sqrt{\frac{g(\rho_{\text{liq}} - \rho_v)}{\sigma_{sf}}} \left(\frac{C_{p,liq} \Delta T_e}{C_{s,f} h_e \text{Pr}^n_{\text{liq}}} \right)^3, \tag{19}$$

where $\Delta T_e = T_w - T_{\text{fluid}}$, μ_{liq} is liquid dynamic viscosity, h_e is phase change enthalpy, g is the gravitational acceleration, ρ_{liq} is liquid density, ρ_v is vapour density, σ_{sf} is surface tension, $C_{p,\text{liq}}$ is liquid heat capacity, h_e is the enthalpy of phase change, and Pr_{liq} is the Prandtl number for the liquid.

To obtain heat flux used in Eqs. (2), (3), (6), and (9) this term is multiplied by the whole inner surface for SNE and the part of inner surface in contact with the bottom part of the fluid for PIM. The model constants C_{sf} and n are assumed to be 0.01 and 1, respectively.

Nonetheless, it has to be acknowledged that the real life process is far more complex and cannot be described by such a straightforward method.

At this point in the modelling of a self-pressurising tank, some placeholder model is needed, providing some alignment with the real process and therefore enabling a better understanding of the investigated system as a whole.

2.3 Comparison of models

It is important to highlight the differences between the models previously described in the literature and the newly developed models.

As regards the simpler models EQ and SNE, the former takes into account two nodes, both of which are in the saturated state, while the latter has only one node, accounting for the two-phase mixture filling the entire volume of the tank. In SNE both liquid and vapour are assumed to have saturation properties.

In the more complex models, ZK and PIM, the former divides the system into three fluid elements (vapour, liquid and a thin, evaporating liquid layer) and two walls elements (one in contact with vapour and one in contact with liquid). PIM divides the fluid into two elements (upper and bottom) and treats the tank wall as a single entity.

Regarding heat and mass transfer within the fluid, ZK calculates the evaporating stream via the thin liquid layer between liquid and vapour, with heat flux driving the mass transfer.

In PIM, the rising mass formula is used; this is independent of the heat transfer between nodes and is driven by the state of the bottom node.

Finally, equations are solved for different sets of unknowns. In PIM these are single pressure, top and bottom enthalpy, volumetric share of the upper part α_u and a single tank wall temperature, a total of five unknowns. The ZK model uses a single pressure, vapour and liquid temperature and mass and two wall temperatures, a total of six unknowns.

The approach to heat transfer differs significantly. Both ZK and EQ models divide the tank walls into two separate entities and account for the temperature difference and heat transfer between them. Furthermore, ambient temperature is taken into account as heat transfer from outside into the tank walls is also considered.

The heat exchange between ambient air and the outer tank walls, for both newly developed models, was assumed to be driven by natural convection. The whole volume of the tank walls was assumed to have the same temperature. Heat transfer between fluid and walls was calculated assuming nucleate boiling in parts in contact with either fluid or two-phase mixture, and using natural convection in parts in contact with vapour.

2.4 Validation method

Pressure was selected as the key initial parameter, as its measurements tend to be most accurate. Based on initial pressure from the selected experimental case, initial temperature was calculated, taking into account the initial mass of nitrous oxide. Next, initial densities, enthalpies and void fraction were calculated. For each run of the numerical experiment, start and end time are declared. The total time set, divided by the set number of steps, determines the number of calculation steps.

Both initial value problem are solved with Runge-Kutta 4th order numerical method. This approach enables all required properties to be calculated effortlessly. The simulation run is stopped when the set end time is reached or when the pressure within the tank reaches the lower end of the range of applicability of parameters from thermophysical database, set here to 0.15 MPa. The models, numerical methods and thermodynamic functions were all implemented within an original Fortran 90 program.

To assess the accuracy and usability of the proposed models, the numerical results were compared with experimental data from two sources: the experiments of Zilliac and Karabeyoglu experiment [11] and Zimmerman *et al.* experiment [12]. These sources were chosen due to the availability of full flow data, i.e. from the start of the process up to the point when the tank pressure reached ambient pressure. If at the final point of the simulation the oxidiser has non-zero gauge pressure, then mass of nitrous oxide within the tank might differ significantly depending on the void fraction of the remaining fluid. Therefore, having access to the characteristics of the whole process enables better accuracy of the comparison by removing ambiguity from the selection of the calculation end condition.

The first set of data used is from [11], where the authors carried out a series of test tank emptying process. The tank had a volume of 0.0354 m^3, and the initial oxidiser mass was varied from 14.59 kg up to 24.12 kg between tests. Based on availability of data, test 1 was chosen for comparison, with an initial mass of 20 kg of N_2O and an initial temperature of 285.5 K (12.35°C). The original authors determined the outflow coefficient C_d of the discharge system after the test, by adjusting the measured and modelled mass flow rates of the liquid. For the test run chosen for comparison herein, C_d was estimated to be 0.425; for other runs it ranged from 0.09 to 0.425. According to the authors, such low values of the flow coefficient suggest the occurrence of cavitation within the piping, reducing the effective size of the flow channels. Pressure, temperature and mass data from this test are available for comparison.

The second set of data featured a transparent polycarbonate tube with metal housing at top and bottom was used. This created a cylindrical tank 0.3556 m long, having an internal diameter of 0.0254 m and 0.00635 m wall thickness, resulting in an internal volume of $1.803 \cdot 10^{-4}$ m^3, capable of holding around 0.14 kg of nitrous oxide.

Outflow was controlled by setting a ball valve, placed in the bottom part of the housing. For a given test, the tank was filled up to a desired level, specified as the fill level, and allowed to reach equilibrium state. Next the valve was opened to a given setting and fluid was evacuated into the atmosphere. Both nitrous oxide and carbon dioxide were tested, although for purposes of model validation, only the nitrous oxide results are used.

Fluid mass flow rate was not directly measured, due to the difficulty of measuring the mass flux of a two-phase flow. Instead, average mass flow was calculated using the initial and final mass of the tank and the time required for emptying.

The lack of accurate measurement of the mass flow is also an issue in assessing the quality of the tank model. Outflow is, by far, the largest factor impacting the behaviour of a self-pressurising tank, and its accurate representation therefore has a significant impact on a model's results. However, the creation of a model predicting the mass flow rate of a two-phase fluid is not an easy task. We consider as an example the SPI-HEM (single phase incompressible – homogeneous equilibrium model) proposed by Dyer [19], including features of homogenous equilibrium two-phase flow and single-phase incompressible flow. The equations used are:

$$\dot{m}_{\text{out}} = \frac{k\dot{m}_{\text{SPI}} + \dot{m}_{\text{HEM}}}{1+k}\,, \tag{20}$$

$$\dot{m}_{\text{SPI}} = C_d A \sqrt{2\rho_1 (P_1 - P_2)}\,, \tag{21}$$

$$\dot{m}_{\text{HEM}} = C_d A \rho_2 \sqrt{2(h_1 - h_2)}\,, \tag{22}$$

$$k = \sqrt{\frac{P_1 - P_2}{P_1^s - P_2}}\,, \tag{23}$$

where k is a weight parameter, C_d is the discharge coefficient, A is the injector cross-sectional area, ρ_1 is the fluid density upstream to the injector, ρ_2 is the fluid density downstream to the injector, P_1 is the pressure upstream to the injector, P_2 is the pressure downstream to the injector, h_1 is the enthalpy upstream to the injector, h_2 is the enthalpy downstream to the injector and P_1^s is the saturation pressure for upstream conditions.

According to the authors, this approach provides an accuracy of +/− 15%. This model was used in [10] to model mass outflow. To circumvent the issue of comparing different injector and feed line systems, an adjusted C_dA parameter was used, tuned to obtain the same emptying time for all the models compared. This makes it possible to minimise the impact of the injector model on the tank model. A similar approach is used in the present investigation. Dyer's model is included in both tank behaviour models, with the C_dA parameter adjusted to fit the experimental emptying time.

3 Results

Data available from the literature were used to recreate the experiments in the simulations. Parameters unavailable from the experiments but required by the models were set to values resulting in the best recreation of the initial experimental conditions. The parameters used for calculations of the first test case are given in Table 1.

Table 1: Summary of the key parameters used for calculations of the Zilliac test case.

Test case	Parameter name	SNE	PIM
Zilliac	Initial temperature	289.2 K	287.85 K
	Initial void fraction	0.375	0.410
	Limit void fraction	1.0	0.99
	CdA	$7.5 \cdot 10^{-5}$	$7.5 \cdot 10^{-5}$
	Time step	1 ms	0.15 ms

For the PIM, the initial void fraction α was adjusted by setting the initial bottom enthalpy h_b as a fraction of liquid saturation enthalpy h_l^s, which means that in the initial state the bottom element has enthalpy lower than saturation, and therefore some energy transfer to the bottom node is needed to bring it to saturation. This enables numerical recreation of the initial sudden pressure drop. Whether the same physical phenomenon causes this pressure drop in the experiments, is an open question. Due to features of the SNE model, the same approach was not needed. For SNE, the initial void fraction α is calculated directly from initial mass and pressure. Differences between the models necessitated a difference in the initial temperatures, which were adjusted to produce saturation pressure equal to the initial experimental pressure values. Temperature adjustment to match initial pressure was also used in the previously reported studies, in view of the

higher accuracy and lower uncertainty of the pressure measurement over temperature measurement [5].

The first set of plots shows results from the newly developed models in comparison with the experimental results published by Zilliac. Figure 3 shows a pressure-time history plot during tank emptying. PIM predicts a sudden, initial pressure drop which is significantly faster than the observed drop. During drainage of the bottom part, it accurately matches the experimental data, predicting a smooth decrease in pressure up to the inflection point. This point represents moment where all of the bottom mass has been drained, and flow transitions to one dominated by vapour. Afterwards, the rate of pressure drop increases significantly until all available nitrous oxide is drained. As for the SNE model, it does not predict any rapid changes, although it captures the overall trend of the process.

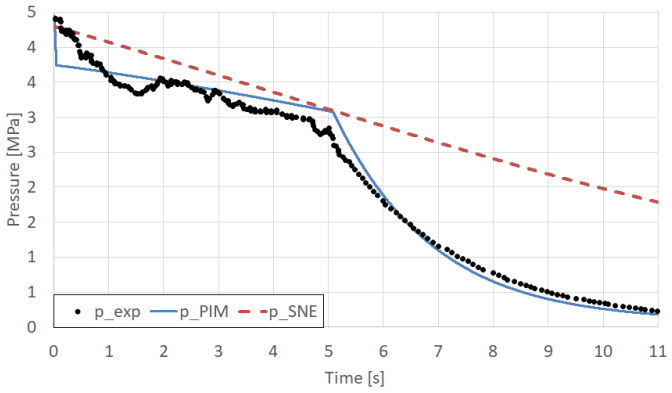

Figure 3: Pressure comparison between Zilliac experimental data and PIM and SNE models.

Figure 4, depicting the volumetric void fraction α, shows the previously mentioned inflection point in the PIM results, where α reaches the limiting value (set herein to 0.99), meaning that all of the mostly liquid bottom part is drained. As before, changes in the SNE model are smoother and less rapid. The difference in the initial values of α results from differences in the models. Both models use pressure as the key initial parameter adjusted to the experiment. For SNE, this is directly correlated with temperature, while for PIM, pressure is affected by the initial temperature and initial void fraction. It is important to note that the values of α from the two models cannot be directly compared, due to differences in modelling. In the SNE model, α represents the total volumetric share of vapour within

the tank, while for PIM, α – as one of model unknowns – describes the volumetric share of the upper part. This difference is a direct result of differences in the models' assumptions. For SNE, there is no division into two elements, only one node with possibility of vapour content. For PIM, each of two separate elements can exist in non-saturated state; the upper, initially vapour element may contain liquid, and the bottom, initially liquid element may contain vapour. The volumetric share of vapour within the bottom element is shown by a dotted line. The volume of vapour within the bottom element is seen to rise steadily up to approx. 0.5 (or 50% by volume) when all of the bottom mass is drained.

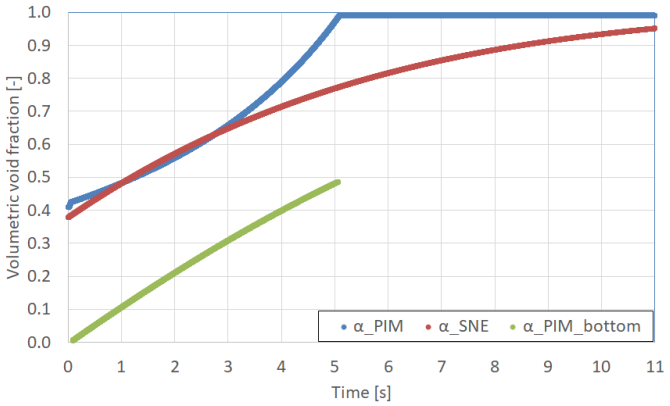

Figure 4: Comparison of volumetric void fraction α between PIM and SNE models for the Zilliac test case.

Figure 5 presents temperature results for both models. No experimental results were available for comparison for this particular case. Nonetheless, temperatures in self-pressurising systems tend to follow a pressure curve as observed in the experiments [12]. It can be inferred that temperature should decrease steadily during the first 5 s of the flow, and inflection point of the curve should be observed after this initial steady decline. After this point, the rate of temperature drop is expected to increase and follow an exponential trend.

Finally, Fig. 6 shows a comparison of nitrous oxide mass within the tank during emptying for both models and for the experiment. During most of the simulation, PIM overestimates mass, and therefore the mass outflow is being underestimated. The SNE model achieves good accuracy within the first four seconds of the process, but this is lost in the transition region, from the first phase of the flow in which mostly liquid is flowing, to the

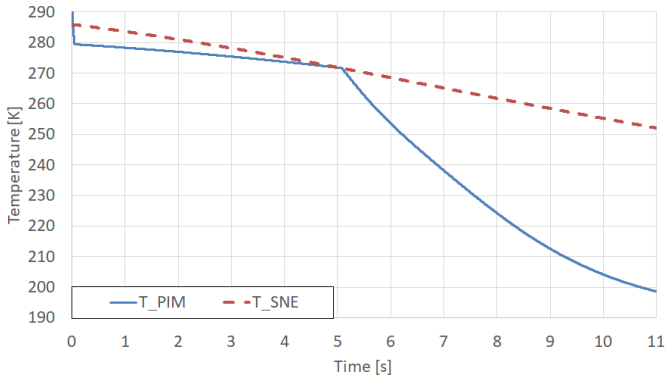

Figure 5: Temperature comparison between PIM and SNE models for Zilliac test data.

second phase with flow mostly consisting of vapour. Similarly as in the previous plots, SNE predicts a smoother process with less rapid changes.

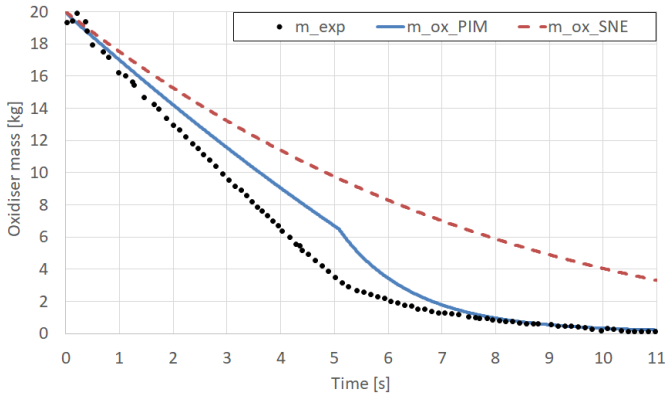

Figure 6: Nitrous oxide mass within the tank for Zilliac experimental data and for PIM and SNE models.

The key parameters used to calculate the second test case are given in Table 2. The overall characteristics of the numerical results in the Zimmerman test case are similar to those of the previous test case. Figure 7 shows the pressure values. For PIM, it is seen that the initial pressure drop is significantly smaller than in the previous case. Pressure values in the first phase of the process have good accuracy, although the duration of that phase is overestimated, with the inflection point calculated at around 13 s, while in the experiment the transition occurred after around 8.5 s. The SNE model,

Table 2: Summary of the key parameters used for calculations of the Zimmerman test case.

Test case	Parameter name	SNE	PIM
Zimmerman	Initial temperature	280.5 K	282.9 K
	Initial void fraction	0.113	0.120
	Limit void fraction	1.0	0.99
	CdA	$1.9 \cdot 10^{-7}$	$1.9 \cdot 10^{-7}$
	Time step	1 ms	0.15 ms

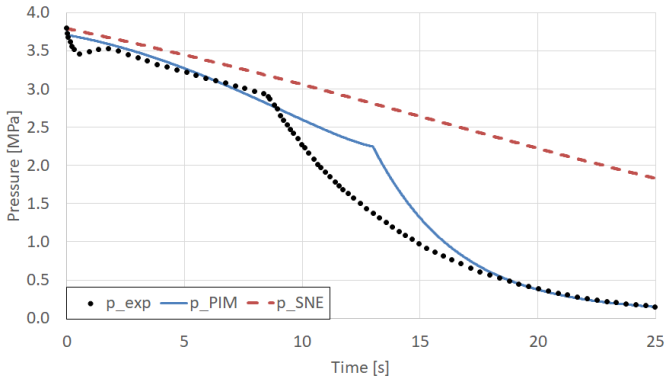

Figure 7: Pressure comparison between Zimmerman experimental data and PIM and SNE models.

as previously, predicts a smooth and featureless pressure drop across the whole simulation time.

Figure 8 shows results for the volumetric void fraction. Similarly to the previous case, the global void fraction rises steadily for SNE model, while for PIM the increase is slower initially and accelerates significantly during the process. Additionally, the volumetric share of vapour within the bottom element is shown by a dotted line labelled α_PIM_bottom. This value increases steadily over time and reaches approx. 0.6 when all of the bottom mass is drained.

Temperatures calculated by the models compared with the experiment are shown in Fig. 9. The temperature results the resemble pressure results, apart from a rise in temperature starting at 15 s. The authors of the original study did not comment on the rise in temperature unaligned with the pressure results. Since the rise is observed only in the temperature mea-

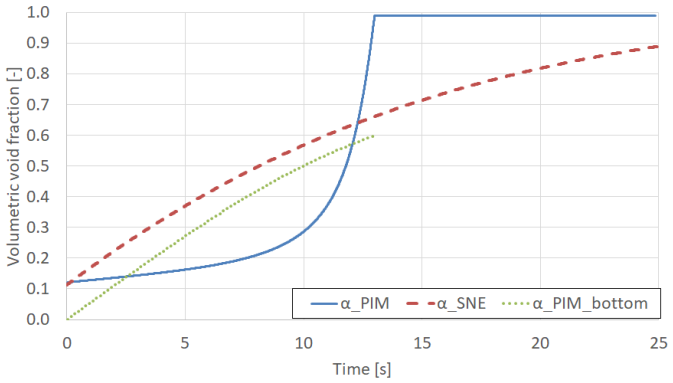

Figure 8: Comparison of the volumetric void fraction α between PIM and SNE models for the Zimmerman test case.

surement, it is most likely linked to either sensor malfunction or a sudden increase in heat flow to the tank. Such an increase in heat flow might have been caused by an increased flow of warm air around the tank. Due to the low mass of nitrous oxide within the tank at the final stage of the experiment and the relatively low heat capacity of the polycarbonate tank, even moderate heat influx might have affected the results. No concrete data supporting these possibilities are available, and therefore the phenomenon could not be recreated using the numerical models.

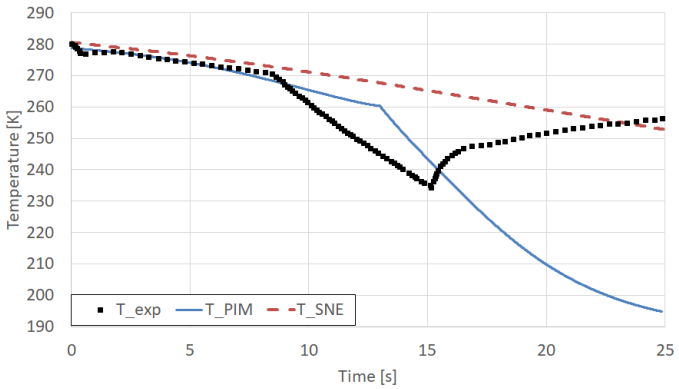

Figure 9: Temperature comparison between Zimmerman experimental data and PIM and SNE models.

Finally, the simulated mass of nitrous oxide within the tank calculated by both models is shown in Figure 10. The trend is similar to the first

comparison case, although accuracy cannot be assessed as the oxidiser mass from this experiment is not available.

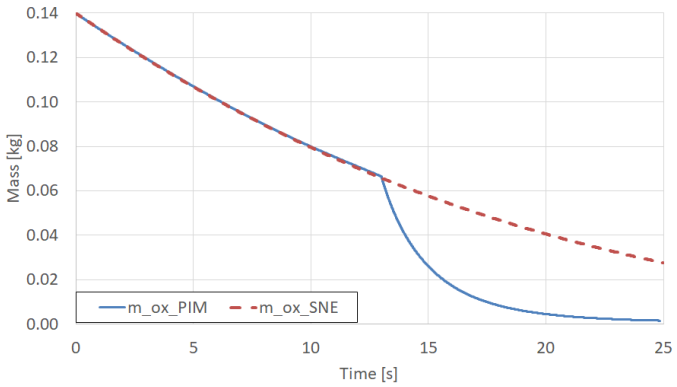

Figure 10: Nitrous oxide mass within the tank for PIM and SNE models for the Zimmerman test case.

4 Discussion

In general, both pressure and temperature results follow the same pattern: an initial sudden drop, followed by an increase and a steady decrease until the curve inflection point, or the transition from liquid-dominated to vapour-dominated outflow [12]. The same pattern has been observed in other experiments featuring self-pressurising tanks, such as those reported in [11] or [12].

None of the models described, either from the literature or the newly developed models, is able to recreate experimental pressure and temperature curves in full. The SNE model is able to predict just a general trend, represented by steady decline of both pressure and temperature. PIM offers more detail, showing the initial drop and change of slope when flow regime changes, but is unable to predict the rise of both pressure and temperature occurring after the initial drop. Furthermore, accurate prediction of the timing of the inflection point (change of slope point) proves to be difficult. For the first presented test case (Zilliac) the PIM model was able to pinpoint this transition in flow behaviour with an accuracy better than 0.2 s, with a total flow time of 11 s. For the second test case (Zimmerman) the timing of the predicted inflection point differs from the experimental value by more than 3 s, out of a total 25 s of the process.

4.1 Accuracy assessment

By comparing the numerical results with the experiments, the qualitative accuracy of the models can be assessed, based on whether general trends or features such as the change of slope of the pressure curve are accurately predicted. Additionally, it is beneficial to use a quantitative measure, especially useful for comparing the performance of various models. To achieve that, the results of the newly developed PIM and SNE models as well as the models developed by Zilliac and Karabeyoglu [11] were compared against experimental data, shown previously as the Zilliac test case. Two variants of the ZK model are shown, with or without evaporation between nodes, denoted here as $\mathrm{ZK}_{\mathrm{evap}}$ and $\mathrm{ZK}_{\mathrm{no\_evap}}$. Due to lack of access to the original experimental and numerical data, the values needed were approximated from graphs provided in the original paper. Pressure plots are shown in Fig. 11. PIM and ZK with evaporation models are performing significantly better than ZK without evaporation and SNE models. SNE is the only model that does not predict a change in behaviour during tank emptying, which is to be expected, since it has only one computational node for the fluid.

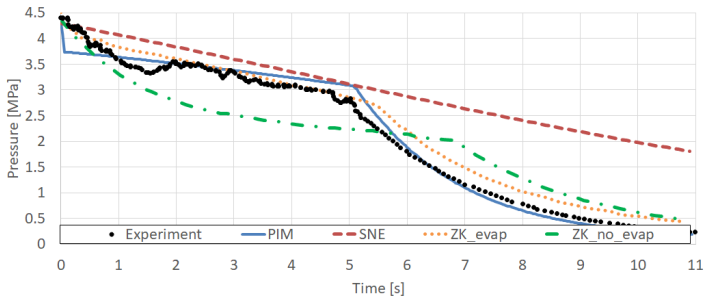

Figure 11: Pressure plot for the investigated models compared with Zilliac's experimental data.

Absolute and relative errors of pressure prediction were calculated for the whole duration of the experiment, as well as one aggregated measure, mean absolute error (MAE), which was calculated using the formula

$$\mathrm{MAE} = \frac{\sum_{i}^{N} |\mathrm{error}_i|}{N}, \tag{24}$$

where the error at a given time step i is

$$\text{error}_i = P_{\text{exp}}(t = i) - P_{\text{model}}(t = i), \tag{25}$$

where P_{exp} and P_{model} are pressure values from the experiment and the model, and N is the number of measurement points for the given model.

Calculated values of MAE are shown in Table 3. It is clear that the PIM and ZK_{evap} models offer the highest accuracy, both being much more accurate than ZK without evaporation modelled and SNE. Overall, PIM has the lowest mean error, lower by 0.071 MPa than the value for ZK with evaporation.

Table 3: Comparison of mean absolute errors for the investigated models.

Model	PIM	SNE	ZK_{evap}	$\text{ZK}_{\text{no evap}}$
Mean absolute error [MPa]	0.136	0.930	0.207	0.475

4.2 Parameter sensitivity

The impact of selected model parameters on the behaviour of the PIM was investigated based on the Zilliac test case. All other model parameters and initial values remained constant. First, Fig. 12 shows pressure values obtained from simulations with two different variants of the initial vapour fraction. The first version, with $\alpha_0 = 0.41$, corresponds to fully saturated liquid in the bottom element. The second version with $\alpha_0 = 0.38$ represents a case where the bottom element has enthalpy lower than that of saturated

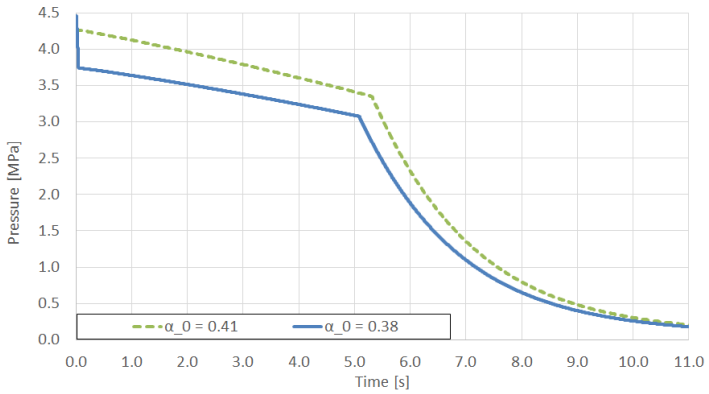

Figure 12: Pressure plots for two variants of initial void fraction.

liquid. It is clearly visible that reducing the initial bottom enthalpy causes a decrease in the initial void fraction and an increase in initial pressure. There is a rapid decrease in pressure during the very beginning of the process. Using saturation conditions in the bottom element results in a smoother process with a minor delay in the transition to mostly vapour flow. Adjustment of this parameter was used here as a means to recreate the experiment as closely as possible. Whether the approach used has a basis in the real process is a matter for future experimental investigation.

To determine the influence of the choice of the limit void fraction α, that is, the total volumetric void fraction value at which it is assumed that all of the bottom part of the nitrous oxide is drained, simulations were performed in two versions. The results are shown on the pressure plot in Fig. 13. The only difference here is the location of the inflection point, meaning that the transition from the first flow regime to the second occurs earlier. It can be observed that $\alpha = 0.8$ is reached after around 4.1 s, while $\alpha = 0.99$ is reached after around 5.1 s.

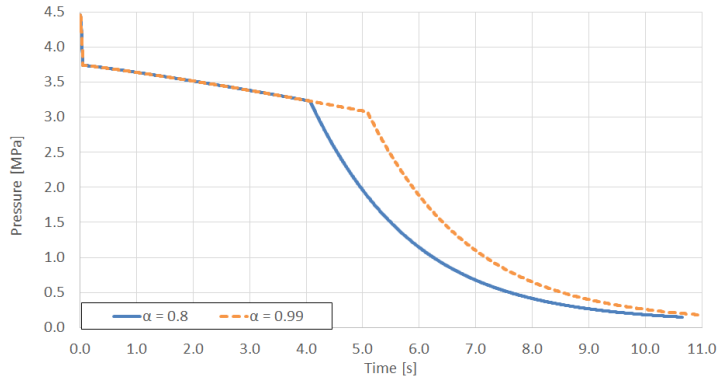

Figure 13: Pressure plot for two different values of limit void fraction.

Furthermore, the importance of mass transported by bubbles rising from the bottom to the upper node was investigated. For this purpose, the same simulation was run twice, once using mass transfer according to Eq. (9), and a second time with the mass source term artificially set to zero. The results are shown in Fig. 14. It is seen that the impact of bubble rising is minor. The pressure plot remains mostly unaffected, with some degree of pressure increase due to this source term. The minor impact might be explained by the value of the rising mass stream, shown in Fig. 15. At maximum, the stream of bubbles for the initial value of the average bubble size of 0.2 mm

reaches 0.021 kg/s. The average mass outflow from the system is equal to 1.71 kg/s, or almost two orders of magnitude higher. Furthermore, after all of the bottom element mass is drained, the rising mass stream is set to zero, as there is no source of vapour bubbles. It can be seen that the rising mass term produced a minor impact on the whole process.

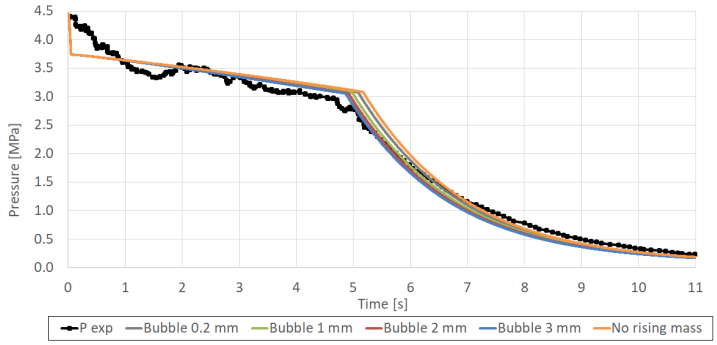

Figure 14: Comparison of pressure plots with and without source term for mass transfer due to rising vapour bubbles.

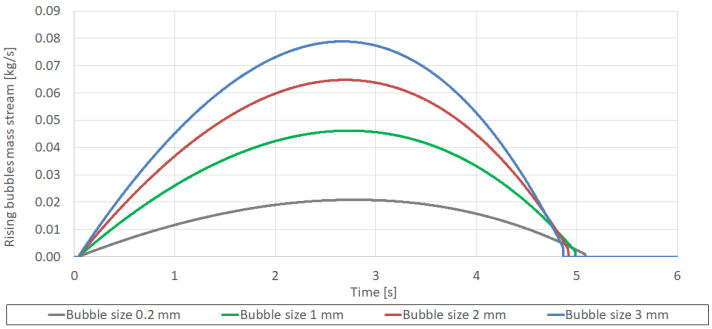

Figure 15: Rising vapour bubbles mass stream for different bubble sizes.

Impact of bubble size on the model was found to be a significant factor and was investigated further. Based on the images available in [12] from test run with valve setting 5, size of some of the bubbles can be estimated due to a known diameter of the transparent tank. Based on the bubbles that could be distinguished, size varied from 1.4 mm to 2.6 mm. Of course only a small fraction of all the bubbles could be properly identified, therefore accurate average size is impossible to determine. Furthermore, it is safe to assume that the bigger bubbles are more visible. Nonetheless, this estimate

allows to identify order of magnitude of the bubble sizes. To investigate impact of this parameter on the model, three trials were conducted, using average bubble size of 1 mm, 2 mm, and 3 mm, respectively. Results of increasing the average bubble size are shown in Fig. 15. Increasing size of the average bubble significantly increases the mass flow due to rising mass. For example, change of size from 0.2 mm to 2 mm changes the maximum flow from 0.02 kg/s, to approx. 0.065 kg/s, or more than threefold. Impact of this change is visible in Fig. 14, showing pressure plots for different bubble sizes and in Fig. 16, also showing pressure, but centred around transition from one flow regime to the other.

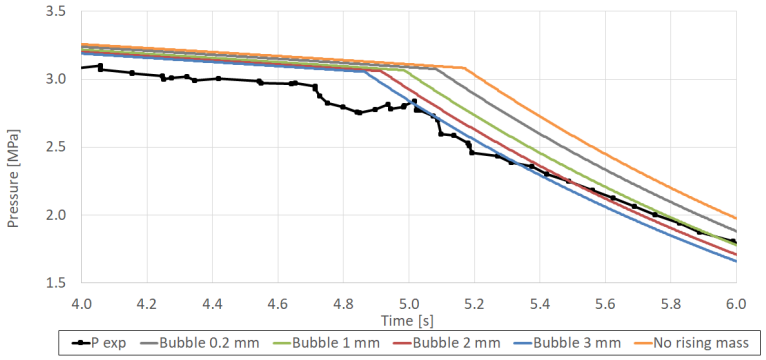

Figure 16: Pressure plots for varying values of the average bubble size, centred around process inflection point.

Changes introduced by the increase of rising mass stream are best visible near transition point, or point where all of the bottom element mass is drained. As expected, increased mass transfer from the bottom to the upper part causes bottom mass to be drained quicker, with difference of approx. 0.2 s between the case with the average bubble size of 0.2 mm and the one with the average bubble size of 3 mm.

Unfortunately, the materials provided in [12] do not permit estimation of the mass or volume of bubbles present. While they seem to be present in most of the volume of the liquid part of medium, the low resolution and lighting of the experimental setup make it unusable for accurate assessment, therefore it is difficult to assess which size of bubble is the most appropriate. Nonetheless, introduction of a parameter with physical meaning to the source term allow for more control of the simulation and better understanding of the physics involved.

5 Conclusions

A major advantage of numerical methods is the possibility of investigation of parameters which are often not possible or not practical to measure. One such parameter is mass transfer between elements of the fluid, represented here as model nodes. A novel source term for rising mass was proposed, using a known relation for bubble velocity within a liquid.

The numerical results show that the proposed term has a minor, but noticeable impact on the global behaviour of the investigated system. At the same time, addition of this mass flow term adds flexibility to the model and may stabilise the modelled system. The rising mass term thus acts similarly to the E parameter used in the ZK model. This parameter enhanced heat flow to boost the evaporative mass stream, while here, direct mass transfer without evaporation at the boundary between nodes can occur, but is taken into account within the bulk of the bottom node. Nonetheless, an experimental investigation would be required to assess the actual impact of both rising and evaporation mass streams, as no assessment of mass transfer between the bottom and upper parts of the self-pressurised tank is currently available.

The SNE model offers a relatively simple and quick tool for predicting the dynamics of a self-pressurised tank with limited accuracy. The PIM model provides a better resolution of the results, enabling the prediction of rapid changes during the process, and usually has better accuracy, at the cost of increased complexity and computational cost.

A characteristic point in the outflow from a self-pressurised tank is the inflection point, determining the transition from liquid-dominated flow to vapour-dominated flow. The SNE model, due to its simplicity, is not able to divide the flow into two parts, while mode detailed models such as PIM or ZK can do this. Accurate prediction of the transition from one flow regime to the other is difficult and depends on selection of model parameters. A crucial parameter is the cut-off point for the vapour fraction within the bottom part, at which it is decided that all of the liquid is drained. The ability to predict the transition is important for the practical utilisation of models, as liquid-dominated flow delivers significantly higher mass flow to the combustion chamber, which translates directly into higher engine thrust.

As for modelling tank mass outflow, a relatively simple Dyer model is used here. For precise determination of flow, both feed line and injector size parameters are needed as well as the state of the fluid within the tank.

Outflow size parameters were adjusted to match experimental data, due to absence of relevant information regarding experimental setups. While the PIM or ZK model can provide a good estimate of fluid parameters within the tank, prediction of the investigated process requires more accurate, detailed knowledge of the outlet elements.

Received 17 January 2022

References

[1] Zilliac G., Waxman B.S., Karabeyoglu A.M., Cantwell B., Evans B.J.: *Peregrine hybrid rocket motor development*. In: Proc. 50th AIAA/ASME/SAE/ASEE Joint Propulsion Conf., 2014.

[2] Rajesh K.K.: *Thrust modulation in a nitrous oxide/hydroxyl-terminated polybutadiene hybrid rocket motor*. In: Proc. 42nd AIAA/ASME/SAE/ASEE Joint Propulsion Conf. Exhibit., Sacramento, 2006.

[3] Tiliakos N., Tyll J., Herdy R., Sharp D., Moser M., Smith N.: *Development and testing of a nitrous oxide/propane rocket engine*. In: Proc. 37th Joint Propulsion Conf. Exhibit., 2001.

[4] Mikielewicz D., Jakubowska B.: *Prediction of flow boiling heat transfer coefficient for carbon dioxide in minichannels and conventional channels*. Arch. Thermodyn. **37**(2016), 2, 89–106.

[5] Scherson Y.D., Lohner K., Lariviere B., Cantwell B., Kenny T.: *A monopropellant gas generator based on* N_2O *decomposition for "green" propulsion and power generation*. In: Proc. 45th AIAA/ASME/SAE/ASEE Joint Propulsion Conf. Exhibit., 2009.

[6] Hennemann L., de Andrade J.C., de Souza Costa F.: *Experimental investigation of a monopropellant thruster using nitrous oxide*. J. Aerosp. Technol. Manage. **6**(2014), 4, 363–372.

[7] Winter A., Marchetta J.: *Simulating self-pressurization in propellant tanks*. In: Proc. 48th AIAA Aerospace Sciences Meet. New Horizons Forum and Aerospace Exposition, Orlando, 2010.

[8] Sanalkumar B.G, Jesna S.B.G.M., Roy K.R.: *Numerical investigation on self pressurisation of cryogenic storage tanks*. Int. J. Sci. Eng. Res. (IJSER) **5**(2014), 7, 897–900.

[9] Casalino L., Pastrone D.: *Optimal design of hybrid rockets with self-pressurizing oxidizer*. In: Proc. 42nd AIAA/ASME/SAE/ASEE Joint Propulsion Conf. Exhib., Sacramento, 2006.

[10] Zakirov V.A., Li L.: *Homogeneous Liquefied Gas Self-Pressurization Model*, In: Proc. Eur. Conf. Aerospace Sciences (EUCASS), 2005.

[11] Zimmerman J.E., Waxman B.S., Cantwell B.J.: *Review and evaluation of models for self-pressurizing propellant tank dynamics*. In: Proc. 49th AIAA/ASME/SAE/ASEE Joint Propulsion Conf., 2013.

[12] Zilliac G., Karabeyoglu M.A.: *Modeling of propellant tank pressurization*. In: Proc. 41st AIAA/ASME/SAE/ASEE Joint Propulsion Conf. Exhibit., 2005.

[13] Zimmerman J.E., Waxman B.S., Cantwell B.J.: *Comparison of nitrous oxide and carbon dioxide with applications to self-pressurizing propellant tank expulsion dynamics*. In: Proc. 60th JANNAF Propulsion Meet., 2013.

[14] Yasuda K., Nakata D., Okada K., Uchiumi M., Higashino K., Imai R.: *N_2O tank emptying characteristics on a running rocket sled*. In: Proc. AIAA Propulsion and Energy Forum, 9-11 July 2018.

[15] Song C., Xu W. Shen C.: *Temperature stratification in a self-pressurized nitrous oxide tank*. J. Propul. Power (JPP) **32**(2016), 2.

[16] Kardaś D., Szymborski J.: *Development of a novel model for emptying of a self-pressurising nitrous oxide tank*. J. Phys. Conf. Ser. **1781**(2021), 1, 1–12.

[17] *NIST Reference Fluid Thermodynamic and Transport Properties — REFPROP*. NIST Standard Reference Database 23, Version 9.1, 2013.

[18] Yefeng Z., Panxing K., Zhengliang H., Pan Y., Jingyuan S., Jingdai W., Yongrong Y.: *Experimental measurement and theoretical analysis on bubble dynamic behaviors in a gas-liquid bubble column*. Chem. Eng. Sci. **211**(2020), 115295–115306.

[19] Bergman T.L., Lavine AS., Incropera F.P., Dewitt D.P.: *Introduction to Heat Transfer*. Wiley, 2011.

[20] Dyer J., Doran E., Dunn Z., Lohner K.: *Modeling feed system flow physics for self-pressurizing propellants*. In: Proc. 43rd AIAA/ASME/SAE/ASEE Joint Propulsion Conf. Exhibit., 2007.

[21] Zimmerman J.E., Cantwell B., Zilliac G.: *Initial experimental investigations of self-pressurizing propellant dynamics*. In: Proc. 48th AIAA/ASME/SAE/ASEE Joint Propulsion Conf. Exhibit., Atlanta, 2012.